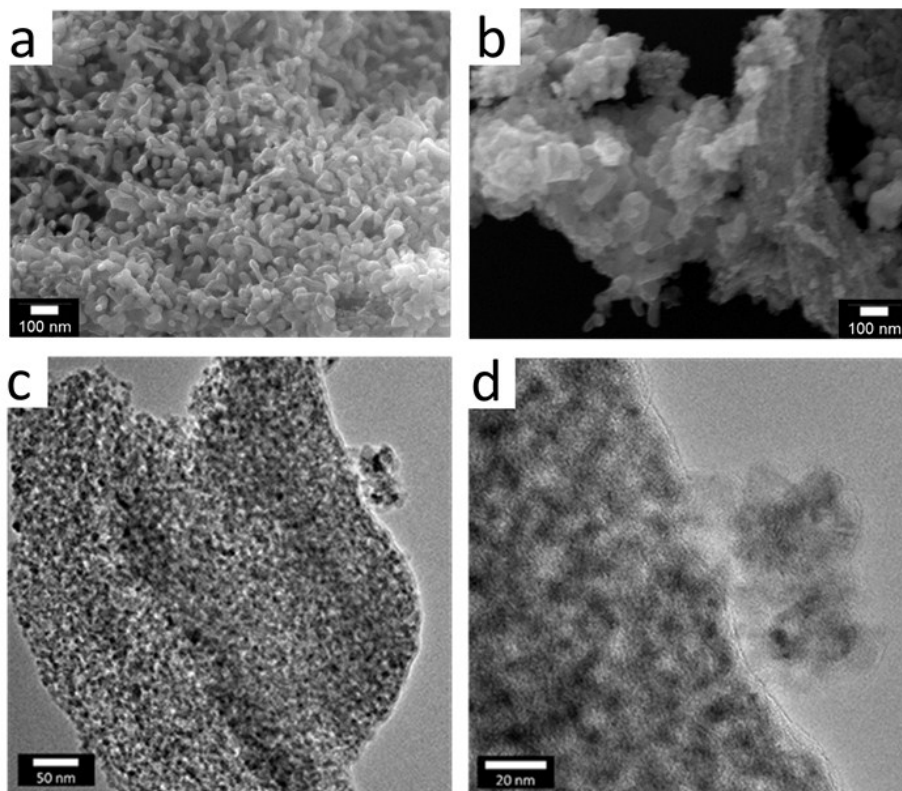


## EXPERIMENTAL SECTION

*Chemicals.* Iron(III) nitrate nonahydrate ( $\text{Fe}(\text{NO}_3)_3 \cdot 9\text{H}_2\text{O}$ ,  $\geq 98\%$ ), iron(III) oxide nanopowder ( $< 50$  nm particle size), glycerol ( $\text{C}_3\text{H}_8\text{O}_3$ , 99.5%), isopropanol ( $\text{C}_3\text{H}_8\text{O}$ , 99.5%), sodium acetate ( $\text{NaCH}_3\text{COO}$ ,  $\geq 99\%$ ), hydrogen peroxide ( $\text{H}_2\text{O}_2$ , 30% w/w in  $\text{H}_2\text{O}$ ), 2,2'-azino-bis (ABTS), terephthalic acid (98%) and absolute ethanol ( $\text{C}_2\text{H}_6\text{O}$ , 99.5%) were purchased from Sigma-Aldrich, Australia. 3,3',5,5'-Tetramethylbenzidine  $\geq 98.0\%$ , was purchased from Sigma Life Science Australia. Dimethyl Sulfoxide AR (DMSO) was purchased from Chem-Supply, Australia. All the chemicals were used as received without further purification.

*Characterization.* All the samples were systematically characterized by various analytical, spectroscopic and imaging techniques. Powder X-ray diffraction (XRD) patterns were obtained by using a Bruker D8 Focus Advance Diffractometer equipped with Lynx Eye detector with a Ni-filtered  $\text{Cu K}\alpha$  radiation ( $\lambda = 1.5406 \text{ \AA}$ ) operating at 40 kV and 40 mA in  $2\theta$  range of 1.0 to 7.0 with a step size of  $0.01^\circ$  and a step time of 2 s. The diffraction patterns were recorded with a divergent slit of  $0.298^\circ$  over the  $2\theta$  range of 1.5 to  $7.5^\circ$  and  $5-50^\circ$  with step size =  $0.01^\circ$  and a step time of 2 s. The lattice parameters were refined by the Rietveld method using the TOPAS program. Transition electron microscopy (TEM) images and selected area electron diffraction (SAED) patterns were obtained by using a 2100 JEOL microscope operated at 120 keV and 200 keV. Prior to the analysis, the samples were ultrasonicated in absolute ethanol for 20 mins and then dropped onto 200-mesh lacey foam coated copper grids and dried at room temperature before loading into the microscope for analysis. Nitrogen adsorption-desorption isotherms were measured at 77 K using Micromeritics ASAP 2020 surface area analyzer. The samples were initially degassed at  $300^\circ\text{C}$  for 4 h before the measurements. Helium was used to carry out free space measurements. The specific surface area was calculated by using the BET (Brunauer-Emmett-Teller) equation, micro- and mesopore-size distribution were obtained from the desorption branch of the isotherm by HK (Horvath-Kawazoe) and BJH (Barrett-Joyner-Halenda) methods, respectively. Diffuse-reflectance ultraviolet and visible spectra of the materials were recorded by using Thermo-Scientific Evolution 600 spectrophotometer (190-800 nm range) with barium sulphate as a standard under ambient conditions. Prior to the analysis, the  $\text{BaSO}_4$  background spectrum was taken followed by the analysis of the samples. Electron paramagnetic resonance (ESR) of the samples was recorded on a Miniflex-II electron spin resonance spectrometer (X-band). The EPR spectra of all the samples were recorded at room temperature with a field modulation of 100 KHz. Magnetization measurements were carried out at 300 K by employing a Lakeshore 7400 vibrating sample magnetometer (VSM). Temperature dependence of magnetization was measured under zero-field cooling (ZFC) and field cooling (FC) with an applied magnetic field of 1000 Oe and temperature range of 10 K to 300 K.

## SUPPORTING FIGURES



**Figure S1.** SEM images of (a) mesoporous  $\gamma$ - $\text{Fe}_2\text{O}_3$  and (b) mesoporous  $\alpha$ - $\text{Fe}_2\text{O}_3$ . (c, d) Enlarged TEM images of mesoporous  $\gamma$ - $\text{Fe}_2\text{O}_3$ .

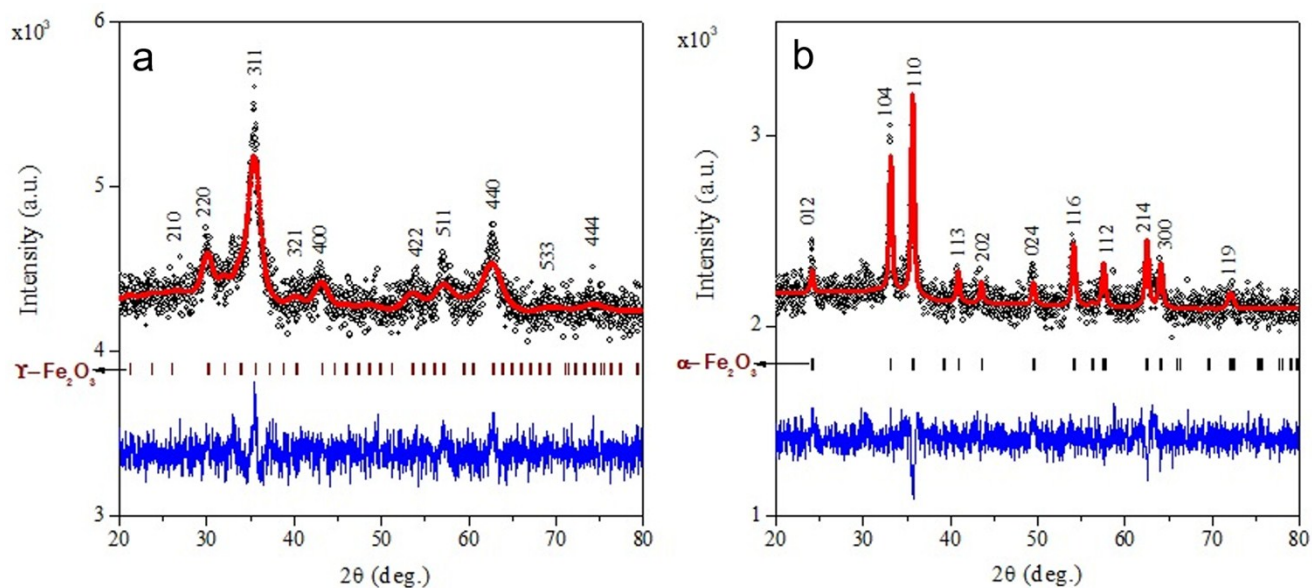


**Figure S2.** Rietveld refined XRD patterns of (a) mesoporous  $\gamma$ - $\text{Fe}_2\text{O}_3$  and (b) mesoporous  $\alpha$ - $\text{Fe}_2\text{O}_3$ . The calculated lattice parameters are  $a, b, c = 8.374(7) \text{ \AA}$  (for mesoporous  $\gamma$ - $\text{Fe}_2\text{O}_3$ ) and  $a, b = 5.0327(9) \text{ \AA}; c = 13.761(3) \text{ \AA}$  (for mesoporous  $\alpha$ - $\text{Fe}_2\text{O}_3$ ), respectively.

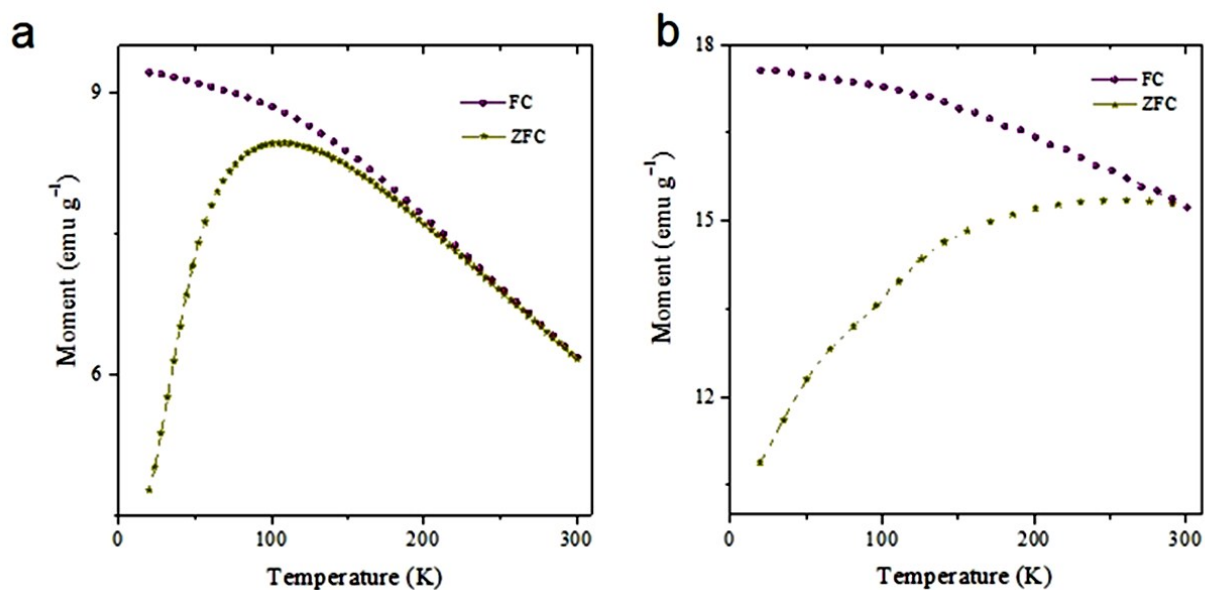


**Figure S3.**  $M$ - $T$  curves of (a) mesoporous  $\gamma$ - $\text{Fe}_2\text{O}_3$  and (b) bulk  $\gamma$ - $\text{Fe}_2\text{O}_3$ .

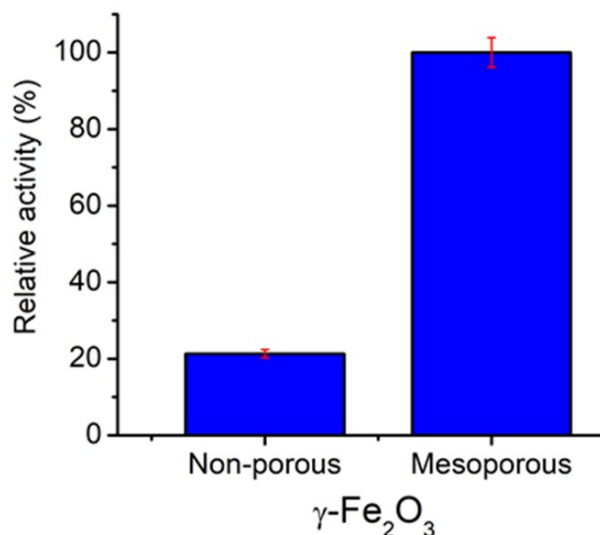


**Figure S4.** The nanozyme activity of non-porous and mesoporous  $\gamma\text{-Fe}_2\text{O}_3$  towards the oxidation of TMB (5  $\mu\text{g}$  NPs, 700  $\mu\text{M}$  TMB, and 500 mM  $\text{H}_2\text{O}_2$  in 0.2 M NaAc buffer; pH = 3.5). Error bars represent the standard error derived from three repeated measurements.

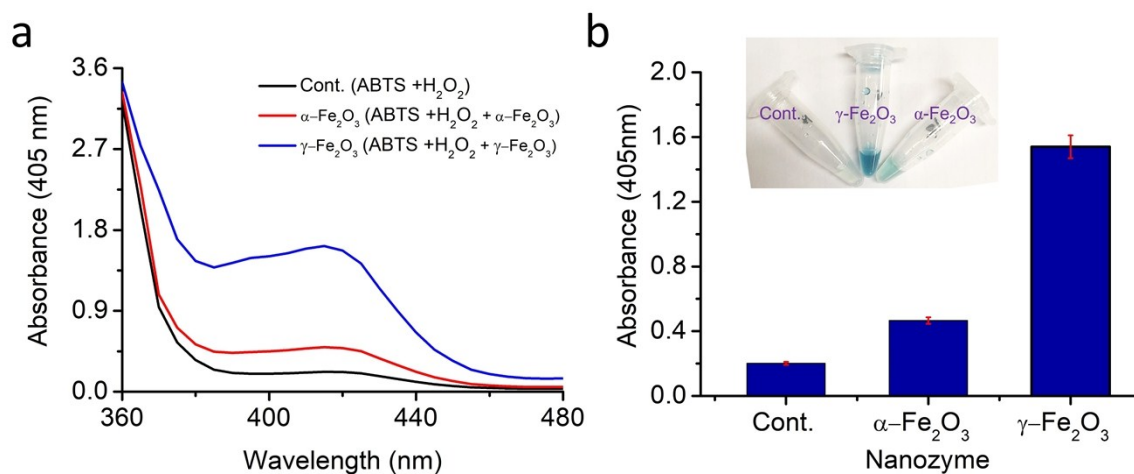


**Figure S5.** (a) The UV-*vis* absorbance spectra obtained for the oxidation of ABTS by peroxidase mimetic activity of iron oxide nanozymes, where the mesoporous  $\gamma\text{-Fe}_2\text{O}_3$  exhibits a much higher nanozyme activity towards ABTS oxidation than the mesoporous  $\alpha\text{-Fe}_2\text{O}_3$ . (b) The corresponding bar diagram for absorbance at 405 nm and the inset shows the color intensity generated by both samples with respect to the control sample (no iron oxide).

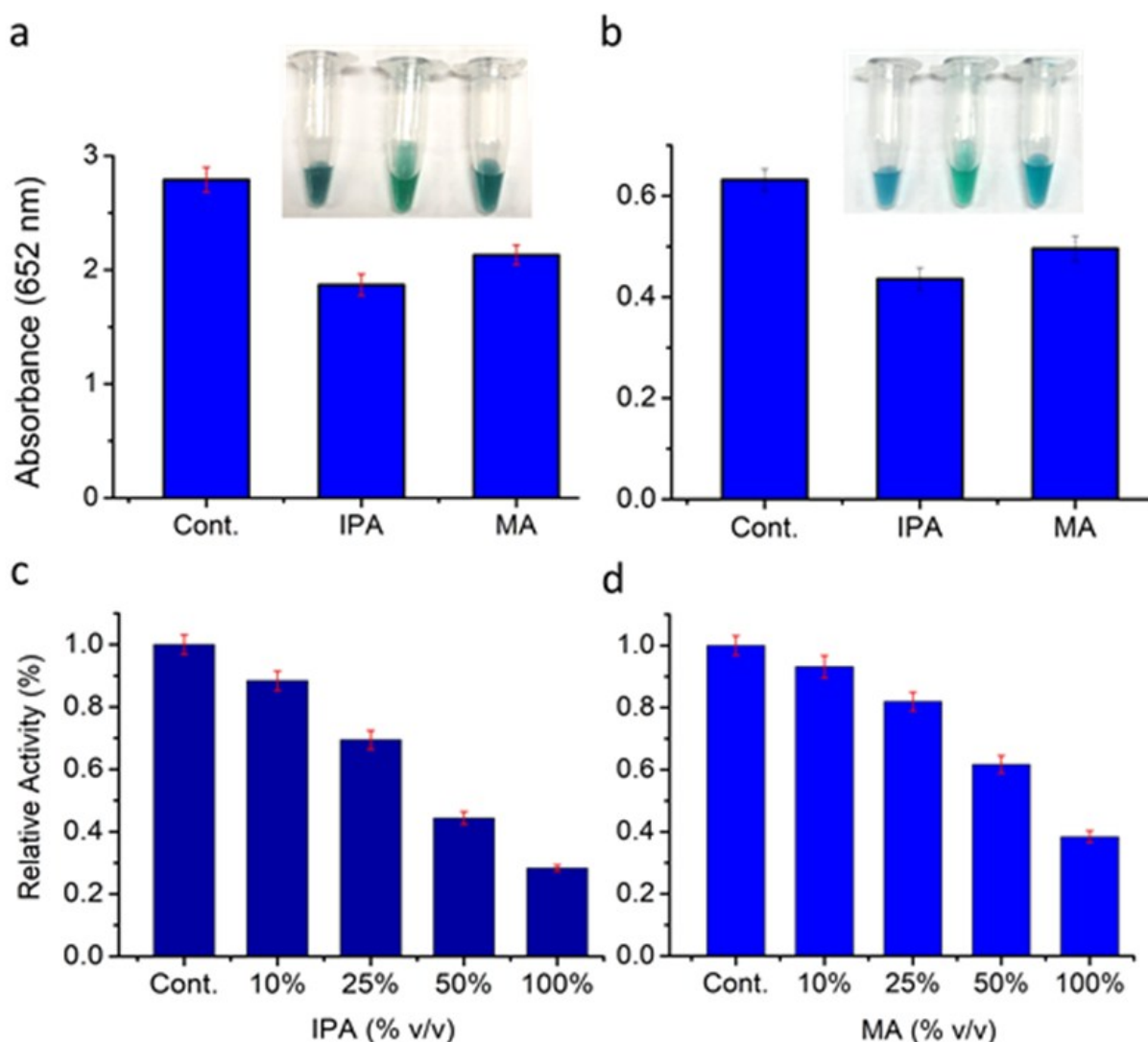


**Figure S6.** (a, b) The responses of absorbance change (at 652 nm) after the addition of hydroxide radical scavengers (isopropanol (IPA) and methyl alcohol (MA)) for both (a) mesoporous  $\gamma\text{-Fe}_2\text{O}_3$  and (b) mesoporous  $\alpha\text{-Fe}_2\text{O}_3$  (TMB<sub>OX</sub>: Scavenger = 1: 0.25). Both IPA and MA scavengers absorb the hydroxyl radical, resulting in lower absorbance than that of the control (cont.) (5  $\mu\text{g}$  of iron oxide in TMB and H<sub>2</sub>O<sub>2</sub> system without any scavengers). Insets show the corresponding images of the color intensity reduction after the reaction with scavengers. (c, d) The absorbance responses after the addition of different amounts of both IPA and MA scavengers towards the mimetic activity of mesoporous  $\gamma\text{-Fe}_2\text{O}_3$ , respectively. With the addition of an equivalent amount of IPA (TMB<sub>OX</sub>: IPA = 1:1), 73 % of hydroxyl radicals is absorbed, where MA absorbs around 62%, leading to the decrease in color intensity as well as absorbance (at 652 nm). Error bars represent the standard error derived from three repeated measurements.

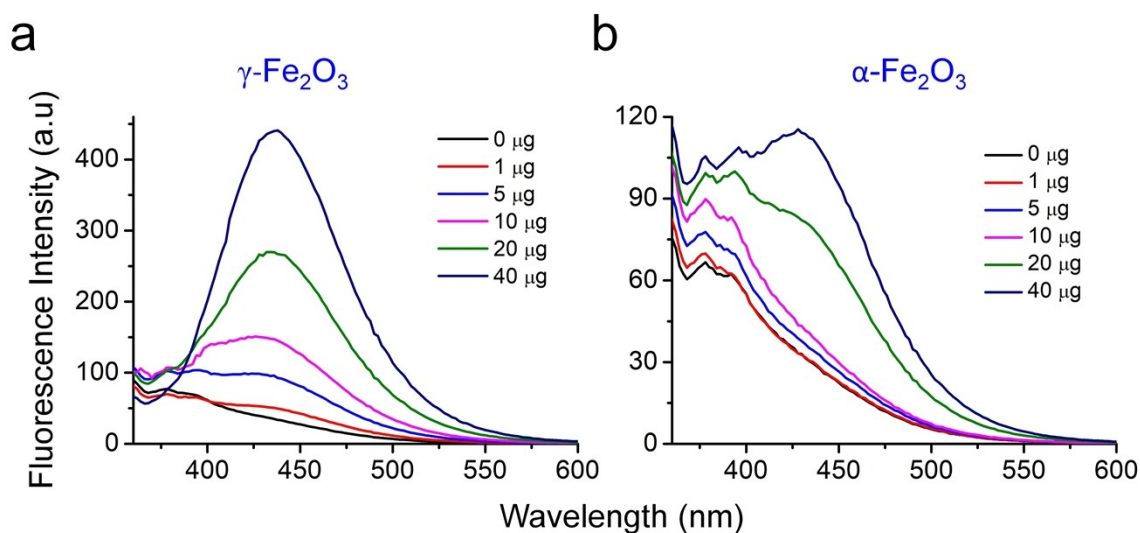


**Figure S7.** Investigation of the hydroxyl ion ( $\cdot\text{OH}$ ) radical formation through the fluorescence spectra of 2-hydroxyterephthalic acid produced from the oxidation of terephthalic acid (TA) by  $\cdot\text{OH}$  in the presence of both (a) mesoporous  $\gamma\text{-Fe}_2\text{O}_3$  and (b) mesoporous  $\alpha\text{-Fe}_2\text{O}_3$ .

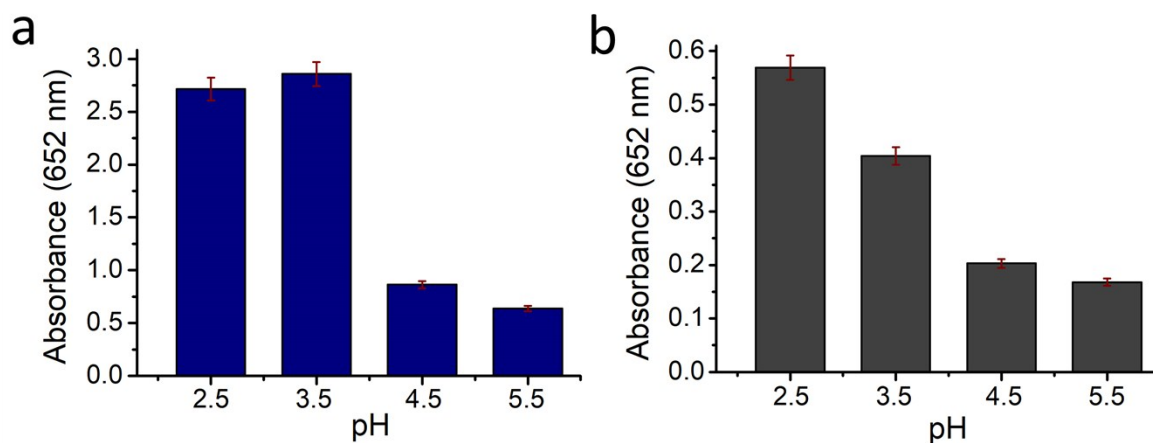


**Figure S8.** The pH-dependent peroxidase-like activities of (a) mesoporous  $\gamma\text{-Fe}_2\text{O}_3$  and (b)  $\alpha\text{-Fe}_2\text{O}_3$  samples (5  $\mu\text{g}$ ). Mean values of absorbance at the designated pH of NaAc (at 25  $^\circ\text{C}$ ) buffer solution. The concentrations of TMB and  $\text{H}_2\text{O}_2$  were 700  $\mu\text{M}$  and 500 mM, respectively. Error bars represent the standard error derived from three repeated measurements.

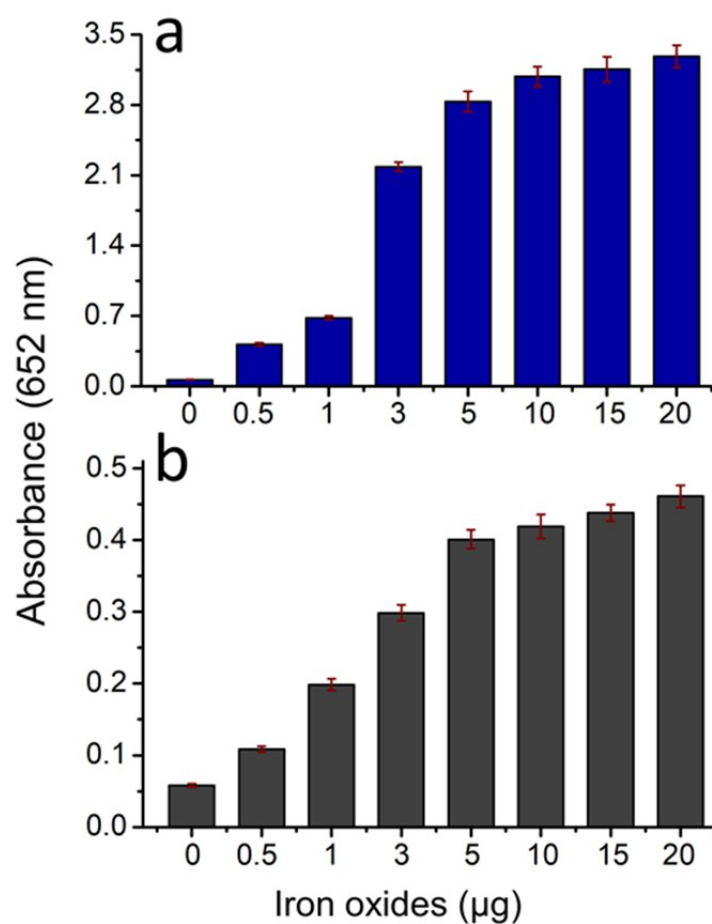


**Figure S9.** The peroxidase-like activities of (a) mesoporous  $\gamma$ -Fe<sub>2</sub>O<sub>3</sub> and (b) mesoporous  $\alpha$ -Fe<sub>2</sub>O<sub>3</sub> samples with different loading amount. Mean values of absorbance obtained with varying quantities of mesoporous iron oxide (0 to 20 μg) in NaAc (at 25 °C) buffer solution with the concentrations of TMB and H<sub>2</sub>O<sub>2</sub> being kept at 700 μM and 500 mM, respectively. Error bars represent the standard error derived from three repeated measurements.

## SUPPORTING TABLE

**Table S1.** Comparison of the peroxidase-mimicking activities (kinetic parameters and conditions) of the as-prepared mesoporous  $\alpha$ -Fe<sub>2</sub>O<sub>3</sub> and  $\gamma$ -Fe<sub>2</sub>O<sub>3</sub> with recently reported iron oxide-based nanostructures and composites for TMB/H<sub>2</sub>O<sub>2</sub> substrate.

Sample	Substrate	$K_m$ (mM)	$V_{max}$ (Ms <sup>-1</sup> )	pH	Temp. (°C)	Reference
Mesoporous $\gamma$ -Fe <sub>2</sub> O <sub>3</sub>	TMB	0.0997	$5.20 \times 10^{-7}$	3.5	25	This work
	H <sub>2</sub> O <sub>2</sub>	144.30	$1.84 \times 10^{-8}$			
Mesoporous $\alpha$ -Fe <sub>2</sub> O <sub>3</sub>	TMB	0.5304	$5.43 \times 10^{-8}$	4	40	[S1]
	H <sub>2</sub> O <sub>2</sub>	127.92	$3.77 \times 10^{-8}$			
Horseradish peroxidase (HRP)	TMB	0.434	$10.0 \times 10^{-8}$	4.5	40	[S2]
	H <sub>2</sub> O <sub>2</sub>	3.7	$8.71 \times 10^{-8}$			
N-doped porous carbon nanospheres (N-PCNSs)	TMB	0.135	$6.13 \times 10^{-8}$	3.5	25	[S3]
	H <sub>2</sub> O <sub>2</sub>	161	$11.7 \times 10^{-8}$			
Iron oxide nanoflakes (C@250 °C)	TMB	0.298	$8.71 \times 10^{-8}$	3.5	25	[S4]
	H <sub>2</sub> O <sub>2</sub>	146.7	$10 \times 10^{-8}$			
Mesoporous Fe <sub>2</sub> O <sub>3</sub>	TMB	0.29	3.9	4	40	[S5]
	H <sub>2</sub> O <sub>2</sub>	44.69	2.23			
Au/CeO <sub>2</sub> CSNPs	TMB	0.374	$2.6 \times 10^{-8}$	4	40	[S6]
	H <sub>2</sub> O <sub>2</sub>	54.6	$1.8 \times 10^{-8}$			
ATP-mediated Fe <sub>3</sub> O <sub>4</sub>	TMB	0.307	$1.06 \times 10^{-6}$	4.6	25	[S7]
	H <sub>2</sub> O <sub>2</sub>	323.6	$1.17 \times 10^{-6}$			
Prussian Blue-modified $\gamma$ -Fe <sub>2</sub> O <sub>3</sub>	TMB	0.118	$5.38 \times 10^{-8}$	3.6	45	[S8]
	H <sub>2</sub> O <sub>2</sub>	305	$1.01 \times 10^{-7}$			
Graphene oxide (GO)-Fe <sub>2</sub> O <sub>3</sub>	TMB	0.488	$2.06 \times 10^{-7}$	3.5	35	[S9]
	H <sub>2</sub> O <sub>2</sub>	0.019	$0.17 \times 10^{-7}$			
FeNPs@Co <sub>3</sub> O <sub>4</sub> hollow nanocages	AU	0.036	$1.55 \times 10^{-6}$	7.0	35	[S10]

## REFERENCES

- [S1] L. Gao, J. Zhuang, L. Nie, J. Zhang, Y. Zhang, N. Gu, T. Wang, J. Feng, D. Yang, S. Perrett, *Nat. Nanotechnol.* **2007**, *2*, 577.
- [S2] K. Fan, J. Xi, L. Fan, P. Wang, C. Zhu, Y. Tang, X. Xu, M. Liang, B. Jiang, X. Yan, *Nat. Commun.* **2018**, *9*, 1440.
- [S3] S. Tanaka, M. K. Masud, Y. V. Kaneti, M. J. A. Shiddiky, A. Fatehmulla, A. M. Aldhafiri, W. A. Farooq, Y. Bando, M. S. A. Hossain, Y. Yamauchi, *ChemNanoMat* **2019**, *5*, 506-513.
- [S4] R. Bhattacharjee, S. Tanaka, S. Moriam, M. K. Masud, J. Lin, S. M. Alshehri, T. Ahamad, R. R. Salunkhe, N.-T. Nguyen, Y. Yamauchi, *J. Mater. Chem. B* **2018**, *6*, 4783-4791.
- [S5] S. Bhagat, N. S. Vallabani, V. Shutthanandan, M. Bowden, A. S. Karakoti, S. Singh, *J. Colloid Interface Sci.* **2018**, *513*, 831-842.
- [S6] N. S. Vallabani, A. S. Karakoti, S. Singh, *Colloids Surf. B Biointerfaces.* **2017**, *153*, 52-60.
- [S7] X.-Q. Zhang, S.-W. Gong, Y. Zhang, T. Yang, C.-Y. Wang, N. Gu, *J. Mater. Chem.* **2010**, *20*, 5110-5116.
- [S8] L. Song, C. Huang, W. Zhang, M. Ma, Z. Chen, N. Gu, Y. Zhang, *Colloids Surf. A* **2016**, *506*, 747-755.
- [S9] J. Zhao, W. Dong, X. Zhang, H. Chai, Y. Huang, *Sens. Actuators B.* **2018**, *263*, 575-584.
- [S10] Y.-C. Yang, Y.-T. Wang, W.-L. Tseng, *ACS Appl. Mater. Interfaces* **2017**, *9*, 10069-10077